Applied Catalysis B: Environmental 163 (2015) 573–583

Contents lists available at ScienceDirect

Applied Catalysis B: Environmental

journal homepage: www.elsevier.com/locate/apcatb

NO oxidation by microporous zeolites: Isolating the impact of pore structure to predict NO conversion

Zhanquan Zhang[a,b,c], John D. Atkinson[b], Boqiong Jiang[d], Mark J. Rood[a,b,*], Zifeng Yan[a,**]

[a] State Key Laboratory of Heavy Oil Processing, Key Laboratory of Catalysis CNPC, China University of Petroleum, Qingdao 266580, China
[b] Department of Civil and Environmental Engineering, University of Illinois, 205 N. Mathews. Ave. , IL 61801, USA
[c] College of Mechanical and Electrical Engineering, China University of Petroleum, Qingdao 266580, China
[d] College of Environmental Science and Engineering, Zhejiang Gongshang University, Hangzhou 310012, China

ARTICLE INFO

Article history:
Received 3 April 2014
Received in revised form 23 June 2014
Accepted 24 June 2014
Available online 1 July 2014

Keywords:
NO oxidation
Catalysis
Zeolite
Activated carbon
Transition states

ABSTRACT

Anthropogenic NO_x emissions from stationary sources to the atmosphere continue to be of concern because of their adverse effects on public health and the environment. An alternative method to conventional selective catalytic reduction to reduce the amount of NO_x emissions is oxidation of NO to more soluble NO_2 upstream of an absorption device. Zeolites and activated carbon are effective NO oxidation catalysts, but their oxidation mechanisms are not fully understood. Here, zeolites were evaluated as NO oxidation catalysts experimentally and theoretically to identify preferred pore structures for NO conversion to NO_2 and to show mechanistic similarities to activated carbon fiber-catalyzed NO oxidation. For the 17 zeolites tested here, steady-state NO conversion is not related to their chemical composition (i.e., Si, Al, or P). However, similar to carbonaceous catalysts, steady-state NO conversion mainly depend on the zeolite's physical properties, including the zeolite's cage size, pore width, and pore volume. Zeolites with maximum free sphere diameter (D_{max}) between 4.70 and 6.45 Å, or zeolites with maximum included sphere diameter (D_i) between 5.71 and 7.37 Å, derived from experimental results, are most effective for NO oxidation to NO_2 regardless of the zeolites' channel-to-cage ratio. A mechanism for NO oxidation proceeding through the [ONOONO] transition state (TS) is described here, challenging the reported mechanism that adsorbed $C^*–NO_3$ species are the precursors of NO_2 formation. Void spaces with dimensions similar to or slightly larger (i.e., 7 Å width) than the size of the TS (4.46 Å × 4.67 Å × 6.94 Å, derived from TS calculations) are the most effective spaces for NO oxidation due to strengthened van der Waals interaction between the confined TS and pore walls of the zeolite. Criteria for screening effective zeolites for NO oxidation are proposed based on results for the 17 tested zeolites, and 82 of the 206 available zeolite codes are predicted to be effective with high steady-state NO conversion. Consistent physical geometries of zeolite pore sizes (D_i = 4.70–6.45 Å or D_{max} = 5.71–7.37 Å) and activated carbon fiber pore widths (5–7 Å) provide convincing evidence that such pore sizes are needed to provide efficient steady-state NO conversion. These results may be extended to other categories of microporous materials to choose the most appropriate material for catalytic NO conversion to NO_2.

1. Introduction

Anthropogenic nitrogen oxides (NO_x, as NO and NO_2), mainly emitted from stationary and mobile combustion sources, deteriorate the environment and human health [1]. Acid rain, stratospheric ozone depletion, photochemical smog, secondary particulate matter, and respiratory diseases can all be at least partially attributed to NO_x emissions [2,3]. In China, NO_x emissions were 1.46×10^{10} kg/year in 2010, an increase of 14% from 2009 [4]. More stringent legislation in China [5] and the USA necessitate the development and use of novel, sustainable NO_x control technologies.

Selective catalytic reduction with $V_2O_5–WO_3/TiO_2$ catalysts is the most mature and common NO_x control technology [6,7]. However, adsorption and catalytic oxidation with liquid absorption (COLA) [8–10] are gaining interest because they operate at lower temperatures (<100 °C) and do not require additional reagents (e.g., NH_3). COLA can also be retrofitted into existing power plants. Such

* Corresponding author at: Department of Civil and Environmental Engineering, University of Illinois, 205 N. Mathews. Ave., Urbana, IL 61801, USA.
Tel.: +1 217 3336963; fax: +1 217 3339464.
** Corresponding author. Fax: +86 53286981295.
E-mail addresses: mrood@illinois.edu (M.J. Rood), zfyancat@upc.edu.cn (Z. Yan).

http://dx.doi.org/10.1016/j.apcatb.2014.06.044
0926-3373/

a NO_x control strategy is especially valuable in China because many existing boilers do not have sufficient space to accommodate new SCR systems between economizers and heat exchangers [11].

Activated carbons [12–19], metal-free zeolites [20–24], and metal oxide-impregnated or ion-exchanged zeolites [10,25,26] have been tested as NO_x adsorbents and NO oxidation catalysts. Microporous materials have low NO adsorption capacities (<2 mg g^{-1}) compared to NO_2 (15–60 mg g^{-1}) [27], and NO is up to 20 times less soluble in water than NO_2 [28–30]. Therefore, both adsorption and COLA processes rely on NO oxidation. Moderate to high temperatures (e.g., 300 °C) are required to enhance conversion for metal-catalyzed NO oxidation. However, NO oxidation via metal-free catalysis is more active at lower temperatures, with dependence on the physical (e.g., pore size distribution) and chemical (e.g., surface functional groups and acidity) properties of the catalyst [20–23,31]. For this reason, this research focuses on identifying preferred physical and chemical catalyst properties for metal-free catalyzed NO oxidation.

The first example of zeolite-catalyzed NO oxidation was shown by Richter *et al.* [32] using NH_4-mordenite (MOR) and NH_4-Y. Later, Halasz *et al.* [33] showed NO oxidation over ZSM-5 with varying Si/Al molar ratios, proposing that bridging hydroxyls (Brønsted acids) are active sites for NO oxidation. Liu *et al.* also used ZSM-5 for NO oxidation and reported that such conversion is independent of Si/Al molar ratio. This is important because it allows for water-resistant (high-silica) zeolites to oxidize NO to NO_2. Kinetic analyses also showed that NO oxidation is second order (2.03) in NO concentration ([NO]), with activation energy of −41 kJ mol^{-1}. Liu reported that this reaction follows an Eley–Rideal mechanism where NO_2 is generated from reactions between gaseous NO and adsorbed NO_3 [20–23]. Na *et al.* investigated NO_x adsorption using zeolites with select physical and chemical properties, showing that zeolite 13X has the highest NO_x adsorption capacity among the investigated zeolites. However, relationships between adsorption capacity and the zeolites' properties were not established [24]. Lu *et al.* showed high NO_x adsorption capacity for Ca-β (221 μmol g^{-1} at 40 °C), possibly due to additional CaO adsorption sites and the three-dimensional framework (*BEA) of the β zeolite-catalyzing NO oxidation [10]. Currently, disagreements remain regarding the NO oxidation mechanism over zeolites. The most recent studies, from Artioli *et al.* [31] and Loiland and Lobo [34], revealed that microporous void spaces provide catalytic sites that accelerate steady-state NO conversion by means of transition state (TS) confinement and stabilization. Loiland and Lobo [34] also extended the scope of NO oxidation catalysts to include microporous metal organic frameworks.

There are 206 unique zeolite frameworks and over 1400 zeolite crystals with varying geometric parameters and compositions [35]. Over 5.3 million zeolite structures are feasible, according to calculations in the Bronze database [36]. Hence, the preferred physical and chemical properties of zeolites for NO oxidation should be described more clearly to provide a framework for selecting zeolites that may have high catalytic activity for NO oxidation.

Activated carbon fiber-catalyzed NO conversion depends on the catalyst's physical properties [12,37,38]. Similar studies are important to identify the preferred structure and composition of zeolite catalysts. The mechanisms for activated carbon fiber-catalyzed and zeolite-catalyzed NO oxidation should be compared to broaden the understanding of the NO oxidation mechanism for microporous materials. If NO oxidation by zeolites relies on a narrow range of micropore widths, then similar mechanisms might be applicable to a wider range of materials.

This study experimentally investigates 17 zeolites with select physical structures and chemical composition (i.e., Si, Al, P, Na^+, NH_4^+, H^+ and Ca^{2+}) to identify the impact of the catalysts' properties on steady-state and transient NO oxidation kinetics. Pore structures (channels or cages) that are most active for NO oxidation are identified and the experimental results are extended to describe a reaction mechanism. TS [ONOONO] confinement [39] and micropore (channels or cages) catalysis are proposed to explain differences in NO conversion. Increasing the van der Waals interaction between the TS and pore walls of the zeolite by adjusting the zeolite's void space dimensions and capacity results in notable differences in NO conversion. These results are consistent with a previously described activated carbon fiber-catalyzed mechanism and can be used to predict, in a more general manner, the properties of porous catalysts for NO oxidation to NO_2 and inspire further NO oxidation investigations for other microporous materials.

2. Methods

2.1. NO oxidation apparatus

The NO oxidation reactor is described in detail elsewhere [12,38], but is briefly described here for clarity. Air (99.9995%), nitrogen (99.999%), and certified 1000 ppm_v NO in N_2 were used to generate the gas streams. Mass flow controllers controlled the individual gas flow rates resulting in the specified [NO], [O_2], and total gas flow rate entering the reactor. Temperatures (25 ± 0.4 or 50 ± 0.4 °C) were maintained in an open water bath. NO oxidation was performed in a stainless steel, fixed-bed reactor packed with 0.25 g of dry zeolite (40–60-mesh, Table 1). Unless otherwise noted, the inlet gas stream consisted of 400 ppm_v NO, 10 vol.% O_2, and balance N_2. Total inlet flow rate was 0.1 standard liters per minute (SLPM at 0 °C and 1 atm). A by-pass line to the downstream NO_x detector was used to ensure a stable [NO_x]. After tests, the bypass line was again used to confirm negligible changes in the inlet [NO] (<0.5% change). [NO_x] was continuously measured with a NO–NO_2–NO_x analyzer (Thermo 42i-HL, sampling every 10 s), and blank experiments confirmed that non-catalyzed NO oxidation was minimal (1.6% at 50 °C). Each test was operated for ≧20 h to achieve steady-state outlet [NO] and [NO_2] (change <1 ppm_v h^{-1}). The catalyst's steady-state NO conversion ($[NO]_{conversion}$) was calculated as follows:

$$[NO]_{conversion}\,(\%) = \frac{[NO]_{inlet} - [NO]_{outlet}}{[NO]_{inlet}} \times 100\% \quad (1)$$

where $[NO]_{inlet}$ and $[NO]_{outlet}$ are the inlet and outlet NO concentrations (ppm_v), respectively.

Adsorption capacity of the samples was determined as described elsewhere [37].

2.2. Preparation of ZSM-5 with a controlled range of microporosity and mesoporosity

ZSM-5 with select microporosity and mesoporosity was prepared with alkali-treatment and employed as a NO oxidation catalyst. Procedures for alkali-treatment of ZSM-5 are described elsewhere [41,42]. In this alkali-treatment, 5 g of ZSM-5-c was dissolved in a flask containing 150 mL of deionized water with select concentrations of NaOH (0.2–0.8 mol L^{-1}). After stirring in a water bath at 80 °C for 30 min, the suspension was cooled to room temperature, and the products were obtained after filtration, washing with water, and drying at 100 °C for >8 h. The products are described as ZSM-5-c-X, where X represents the molarity of NaOH. The relative crystallinity was determined based on procedure B described in ASTM d5758-01 [43].

2.3. Description of zeolites' channels and cages

Physical properties of zeolites are classified using the following terminology. Maximum free sphere diameter (D_{max}) represents

Table 1
Tested zeolites and carbon, their suppliers, and compositions.

Zeolites	Supply	Composition/mole ratio	Crystalline[h]
13X	Sinopharm Chemical Reagent Co., Ltd., China	Na^+ form, SiO_2/Al_2O_3 = 2.46	Y
5A	Shanghai Zeolite Co., China	Ca^{2+} form, SiO_2/Al_2O_3 = 2	Y
MCM-41[a]	Prepared in laboratory	Na^+ form, SiO_2/Al_2O_3 = 30	N
SAPO-11[b]	Nankai Catalyst Co., Ltd., China	$SiO_2/Al_2O_3/P_2O_5$ = 0.38:1:0.71	Y
SAPO-5[c]	Prepared in laboratory	$SiO_2/Al_2O_3/P_2O_5$ = 0.2:1:0.97	Y
NaY	Zibo Catalyst Co., China	Na^+ form, SiO_2/Al_2O_3 = 5.6	Y
USY	Zibo Catalyst Co., China	H^+ form, SiO_2/Al_2O_3 = 10	Y
FER	Zeolyst International, USA	NH_4^+ form, SiO_2/Al_2O_3 = 20, CP914C	Y
ZSM-22[d]	Zhuoyue Co., Ltd., China	SiO_2/Al_2O_3 = 62	Y
β-NK	Nankai Catalyst Co., Ltd., China	Na^+ form, SiO_2/Al_2O_3 = 25	Y
β-ZB	Qingdao Yingrui Ind. and Trade, Co., Ltd., China	Na^+ form SiO_2/Al_2O_3 = 25	Y
ZSM-5-a	Lanzhou, China	SiO_2/Al_2O_3 = 388	Y
MOR	Nankai Catalyst Co., Ltd, China	NH_4^+ form, SiO_2/Al_2O_3 = 25	Y
ZSM-5-b	Zeolyst International, USA	NH_4^+ form, SiO_2/Al_2O_3 = 50, CBV5524G	Y
SAPO-34[e]	Nankai Catalyst Co., Ltd., China	$SiO_2/Al_2O_3/P_2O_5$ = 0.6:1:0.837	Y
MCM-22[f]	Prepared in laboratory	SiO_2/Al_2O_3 = 30	Y
ZSM-5-c	Nankai Catalyst Co., Ltd., China	H^+ form, SiO_2/Al_2O_3 = 38	Y
ACFC-10[g]	American Technical Trading, Co., USA	Carbon = 94 wt%	N

[a] MCM-41 is a mesoporous material containing Al that was prepared via alkali-treatment and self-assembly.
[b] SAPO-11 was purchased with the template and then subjected to calcination at 600 °C for 12 h with a ramp of 2 °C min^{-1} in air atmosphere.
[c] SAPO-5 was prepared according to [40].
[d] ZSM-22 was calcined at 350 °C for 1 h, then at 550 °C for 12 h in pure O_2 atmosphere.
[e] As-purchased SAPO-34 was calcined at 350 °C for 1 h, then at 550 °C for 5 h in air atmosphere.
[f] MCM-22 was provided by Tianjin University.
[g] ACFC-10, activated carbon fiber cloth: batch ACC-5092-10.
[h] XRD patterns are provided in supporting information.

the largest spherical molecule that can pass through a zeolite channel along a given crystallographic axis (*a*, *b*, or *c*) [44]. Maximum included sphere diameter (D_i) represents the largest spherical molecule that can fit in a zeolite cage with volume (V_{cage}), assuming the cage is spherical:

$$V_{cage} = \frac{\pi D_i^3}{6} \quad (2)$$

See Supporting Information (Fig. S1) for graphical descriptions of the channels and cages.

2.4. Calculation of volume and dimensional size of transition state [ONOONO] during NO oxidation

The [ONOONO] TS during NO oxidation was first identified by Gadzhiev *et al.* [39] who investigated the reaction of O_2 and NO using *ab initio* wave functional methods. In this research, the volume of this TS was calculated using density functional theory (DFT). These calculations were completed at the B3LYP/6-31G (d) level using Gaussian software (2003) [45]. The structure of TS was optimized using CCSD (T) and CASSCF methods, and the volume of this TS was computed as the volume inside a contour of density 0.001 electrons a_0^{-3}. Dimensions (length × width × height) were measured using visualization software (Chemcraft 1.6). The van der Waals radii for N_2 and O_2 were 1.55 and 1.52 Å, respectively [46], and were used for calculating the TS's dimensions.

2.5. Characterization of zeolites' crystal patterns and porosity

The crystal patterns of zeolites were obtained using X-ray diffraction (XRD, BRUKER D-5000) with Cu Kα radiation, a step size of 0.02°, and a scan range of 5–50° with a scan rate of 2° min^{-1}. Sample porosity was measured with N_2 adsorption on a Micrometrics surface analyzer (Tristar 3000) at −196 °C. Prior to analysis, the samples were degassed at 300 °C for >6 h. Total pore volume was obtained at a relative pressure of 0.98, total surface area was calculated by BET method, and micropore surface area and micropore volume were calculated with the *t*-plot method.

3. Results and discussions

3.1. Temperature-dependent NO conversion

Steady-state NO conversions for the tested zeolites at 25 and 50 °C are described in Fig. 1. ZSM-5-a/b, SAPO-34, MCM-22, ZSM-22, β and MOR oxidize 25–40% of NO at 25 °C, while the other zeolites oxidize <25% of the NO at the same temperature. NO conversions for the most active zeolites (MCM-22 and SAPO-34) at 50 °C are 16.2–17.1%, which are 28–30% of those for activated carbon catalyst (57%, 50 °C) [38]. NO conversion shows a negative temperature dependence for all zeolites except NaY and 13X. This negative dependence of NO conversion on temperatures is attributed to their negative activation energies [20]. This negative trend, which differs from observations for metal oxide-catalyzed NO oxidation, implies that the reaction mechanism may not follow traditional Eley–Rideal or Langmuir–Hinschelwood pathways [47]. Regarding NaY and 13X, lower conversion at lower temperature, indicates an apparent positive activation energy for NaY and 13X-catalyzed NO oxidation. This opposite trend indicates the existence of either a different reaction mechanism and/or the loss of catalytic sites at lower temperatures. For zeolites with a high concentration of $Na^{\pm}$, such as 13X and NaY, Loiland and Lobo [34] proposed an $Na^{\pm}$-mediated pathway that enhances $NO^{\pm}$-adsorbed species during NO oxidation, improving overall conversion. This pathway, however, also has negative activation energy and therefore cannot explain the inverse temperature dependence observed for 13X and NaY. Another possibility is that the high NO_x adsorption capacities of NaY and 13X (1778 and 2043 μmol g^{-1} at 25 °C, respectively), resulting from accessible $Na^{\pm}$ ions located in S_{II} and S_{III} positions [48], cause blockage of microporosity, decreasing conversion at low temperatures more significantly than at higher temperatures [49]. Loiland and Lobo [34] similarly hypothesized this possibility: NO_2 inhibition may have caused microporous spaces to be occupied, altering the catalyst's NO conversion and kinetics at lower temperatures.

3.2. Chemical composition-performance relationship

For all the zeolites, except for ZSM-5-b, FER, MOR, and USY, outlet [NO] immediately decreases (the first local minimum), then

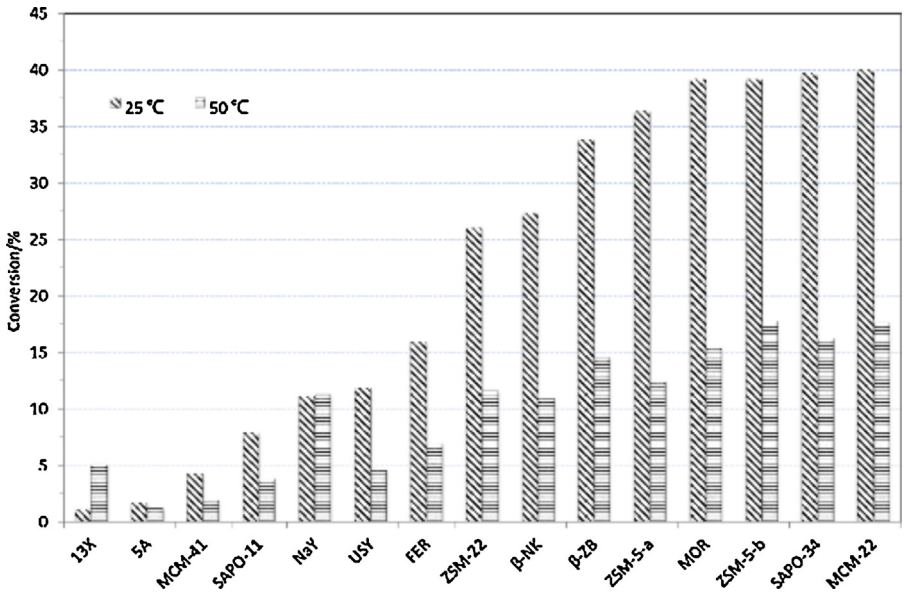

Fig. 1. Steady-state NO conversion over select zeolites at 25 and 50 °C. SAPO-5 and ZSM-5-c were not included because the test at 50 °C did not occur due to the insufficiency of SAPO-5 and ZSM-5-c.

increases (within 60 s, Fig. S3) to a peak before decreasing again to a stable concentration (1 ppm_v h^{-1} change, Fig. S4). The peak in outlet [NO] curve is attributed to NO_2 disproportionation associated with the formation of NO^+ and NO_3^- during NO_2 adsorption with zeolites [50], which is consistent with results for carbonaceous NO oxidation catalysts [37]. Outlet [NO_2] increases to a stable concentration (<1 ppm_v h^{-1} change) after breakthrough (0–35 h, depending on the zeolite) (Fig. S4).

The second local minimum in [NO] is observed for ZSM-5-b, FER, MOR, and USY zeolites. This behavior is not consistent with other NO oxidation catalysts and may be related to the NH_4^+ cations present on these materials. NH_4^+ can cause NO_x reduction, impacting the effluent concentration profiles [32]. By inference, the composition of zeolites, including the presence of cations, may influence transient NO oxidation kinetics, including outlet [NO] and [NO_2] profiles, and the time to achieve steady-state conditions at 25 °C (Fig. 1, Table S1) and 50 °C (Fig. 2, Fig. S5, Table 2). The high NO_2 adsorption capacities of NaY and 13X are attributed to the presence of Na^+, which also increases the corresponding breakthrough time because of strong acid–base interactions [51]. MCM-41 with less Na^+ than NaY and 13X based on the Si/Al molar ratio also has increased NO_2 breakthrough time (and time to achieve steady-state conditions) but less total NO_x adsorption capacity.

In zeolite synthetic chemistry, compensated cations were incorporated into the zeolite matrix to balance the charge brought by aluminum tetrahedrons. The resulting compensated ions, varying with Si/Al molar ratio, can influence transient NO oxidation kinetics as detailed above. However, Si/Al molar ratio is not expected to have same influence on steady-state NO conversion (Fig. 2 and Fig. S5). For example, ZSM-5-a/b/c have similar steady-state NO conversion (36.4–44.0%) despite an order of magnitude range in Si/Al molar ratio. In terms of transient NO oxidation kinetics, more time is required to reach steady-state for ZSM-5-b (Si/Al = 25) and ZSM-5-c (Si/Al = 18) compared with ZSM-5-a (Si/Al = 194), because a lower Si/Al ratio is associated with more compensated cations, which facilitates NO_x adsorption. For steady-state NO conversion, lower Si/Al molar ratio for the ZSM-5 catalysts results in higher conversion, indicating that within a given zeolite framework (i.e., constant D_i and D_{max}, Table 2), Si/Al molar ratio may have an impact on NO conversion. This is consistent with Loiland and Lobo's [34] findings that show cations ($Na^{\pm}$) associated with the introduced Al contribute to NO oxidation. However, this rule should not be applied across all catalysts. MOR (MOR), MCM-22 (MWW), ZSM-5-a/b (MFI), β (*BEA), and SAPO-34 (CHA) have a wide range of Si/Al molar ratios (0.3 to 194) and topologies, however, they all perform effectively (25–40%) once steady-state conditions are achieved [35]. Particularly, 13X and 5A with a Si/Al molar ratio ≤2 show a lower conversion (≤3%), while SAPO-34 with a Si/Al molar ratio of 0.3 has a conversion of 39.8%. That is, lower Si/Al is not expected to have higher conversion, indicating that the influence of Si/Al molar ratio on NO conversion is less significant than that of other factors (e.g., pore volume, pore size, as discussed later). However, the contribution of Si/Al ratio to NO conversion should be identified for a series of zeolites with the same topologies and approximate physical properties in the future.

3.3. Structure–performance relationship

As previously mentioned [12,38], activated carbon fiber cloth's physical properties control the catalyst's steady-state NO conversion [37]. Results to this point demonstrate that the zeolite's chemical properties do not provide consistent impact on the steady-state NO conversion. It is therefore beneficial to investigate the relationship involving steady-state NO conversion and the physical properties of the catalysts. Steady-state NO conversion was plotted against surface area, pore volume, D_{max}, and D_i of the fresh zeolite catalysts that were determined before NO oxidation tests (Fig. 3a–d, respectively).

There is no apparent correlation between micropore and total surface areas or pore volumes with steady-state NO conversion (Fig. 3a and b, respectively). In spite of its large surface area and pore volume, MCM-41 has low NO conversion (4.3% at 25 °C). Also, FER and MOR have nearly identical surface areas and total pore volumes (within 12.8 and 2.5%, respectively), but their NO conversions differ by 59%, indicating that the framework of the zeolite (i.e., the distribution of void space provided by channels and cages) needs to be considered when predicting steady-state NO conversion. These results are once again consistent with studies investigating activated carbon catalysts for NO oxidation—high conversion is not controlled by the bulk physical properties (i.e., surface areas or pore volumes) of the catalyst [12]. A narrow range of pore widths (5–7 Å) were important for activated carbon fibers to achieve larger

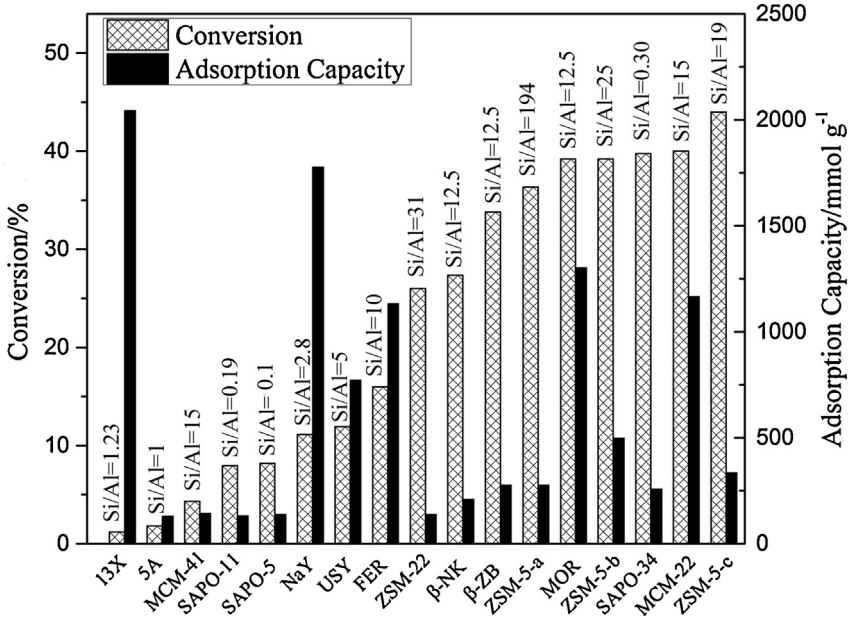

Fig. 2. Relationship between steady-state NO conversion, adsorption capacity, and Si/Al molar ratio for select zeolites (25 °C).

steady-state NO conversion, and such observation should be investigated with zeolites, where void space can be dominated by narrow channels (e.g., MOR, ZSM-22) or large cages (e.g., SAPO-34), or be evenly distributed between the two geometries (e.g., MCM-22) (Table 2). This makes it particularly important to identify individual contributions due to the sizes of the channels (D_{max}) and cages (D_i) rather than relying on bulk properties (i.e., surface area and pore volume, Fig. 3a and b, respectively).

D_{max} identifies the catalyst's channel width and provides an upper limit that prevents or allows gas diffusion into or out of void spaces (sum of channel and cage) (Table 2). The eight tested zeolites with highest steady-state NO conversions (25.0–40.0%), including ZSM-5-a/b (4.70 Å, up to 39%), MOR (6.45 Å, 39%), MCM-22 (4.92 Å, 40%), SAPO-34 (3.72 Å, 40%), β-NK/ZB (5.95 Å, up to 34%), and ZSM-22 (5.11 Å, 26%) (Fig. 3c), have D_{max} values between 3.72 and 6.45 Å. This range of channel widths allows void space to be penetrated by the reactants (NO = 3.17 Å, O_2 = 3.46 Å), while also allowing for the release of the NO oxidation product (NO_2 = 3.40 Å) [52].

Total void space and the distribution of void spaces provided by channels/cages should be incorporated into predictions for steady-state NO conversion by considering more than D_{max} since it represents the smallest width of channels connecting zeolite cages (or the overall, average channel width in zeolites without cages). For example, SAPO-34 has a high steady-state NO conversion (40%). However, because channels contribute <10% of SAPO-34's void space, its strong performance cannot be attributed to its desirable D_{max}. A similar argument is valid for zeolite 5A, which has a low steady-state NO conversion of 1.8% despite its desirable D_{max} value of 4.21 Å. Prediction of NO conversion of zeolite catalysts should be based on more than D_{max}. The appropriate value of D_{max} allows the

Table 2
Topological information and physical properties of select zeolites [44].

Zeolite	Code structure	MR[a]	D_i[b] (Å)	nD[c]	D_{max}[d] (Å)			Total surface area ($m^2\ g^{-1}$)	Micropore surface area ($m^2\ g^{-1}$)	Total pore volume ($cm^3\ g^{-1}$)	Micropore volume ($cm^3\ g^{-1}$)
					a-axis	*b*-axis	*c*-axis				
13X	FAU	12-MR	11.24	3	7.35	7.35	7.35	397	400.0	0.255	0.207
5A	LTA	8MR	11.05	3	4.21	4.21	4.21	379	327	0.276	0.170
MCM-41	N/A	N/A	28	1	N/A	N/A	N/A[e]	872	0	0.749	0[f]
SAPO-11	AEL	10MR	5.64	1	4.63	2.01	2.01	145	134	0.183	0.069
SAPO-5	AFI	12MR	8.30	1	2.22	2.22	7.42	105	65.9	0.065	0.034
NaY	FAU	12-MR	11.24	3	7.35	7.35	7.35	558	521	0.310	0.270
USY	FAU	12-MR	11.24	3	7.35	7.35	7.35	637	559	0.437	0.287
FER	FER	10MR	6.25	2	1.56	3.40	4.69	230	205	0.159	0.107
ZSM-22	TON	10MR	5.71	1	2.31	1.56	5.11	144	156	0.276	0.082
β-NK	*BEA	12MR	6.68	3	5.95	5.95	5.95	470	368	0.310	0.190
β-ZB	*BEA	12MR	6.68	3	5.95	5.95	5.95	416	355	0.406	0.183
ZSM-5-a	MFI	10MR	6.36	3	4.70	4.46	4.46	326	231	0.167	0.120
MOR	MOR	12MR	6.70	1	1.57	2.95	6.45	264	246	0.163	0.127
ZSM-5-b	MFI	10MR	6.36	3	4.70	4.46	4.46	290	238	0.229	0.123
SAPO-34	CHA	8MR	7.37	3	3.72	3.72	3.72	474	486	0.256	0.245
MCM-22	MWW	10MR	9.69	2	4.92	4.92	2.60	415	325	0.347	0.150
ZSM-5-c	MFI	10MR	6.36	3	4.70	4.46	4.46	306	223	0.187	0.116

[a] Member rings.
[b] Maximum included sphere diameter.
[c] Pore dimensions.
[d] Maximum free sphere diameter.
[e] Not applicable.
[f] MCM-41 is a typical mesoporous material.

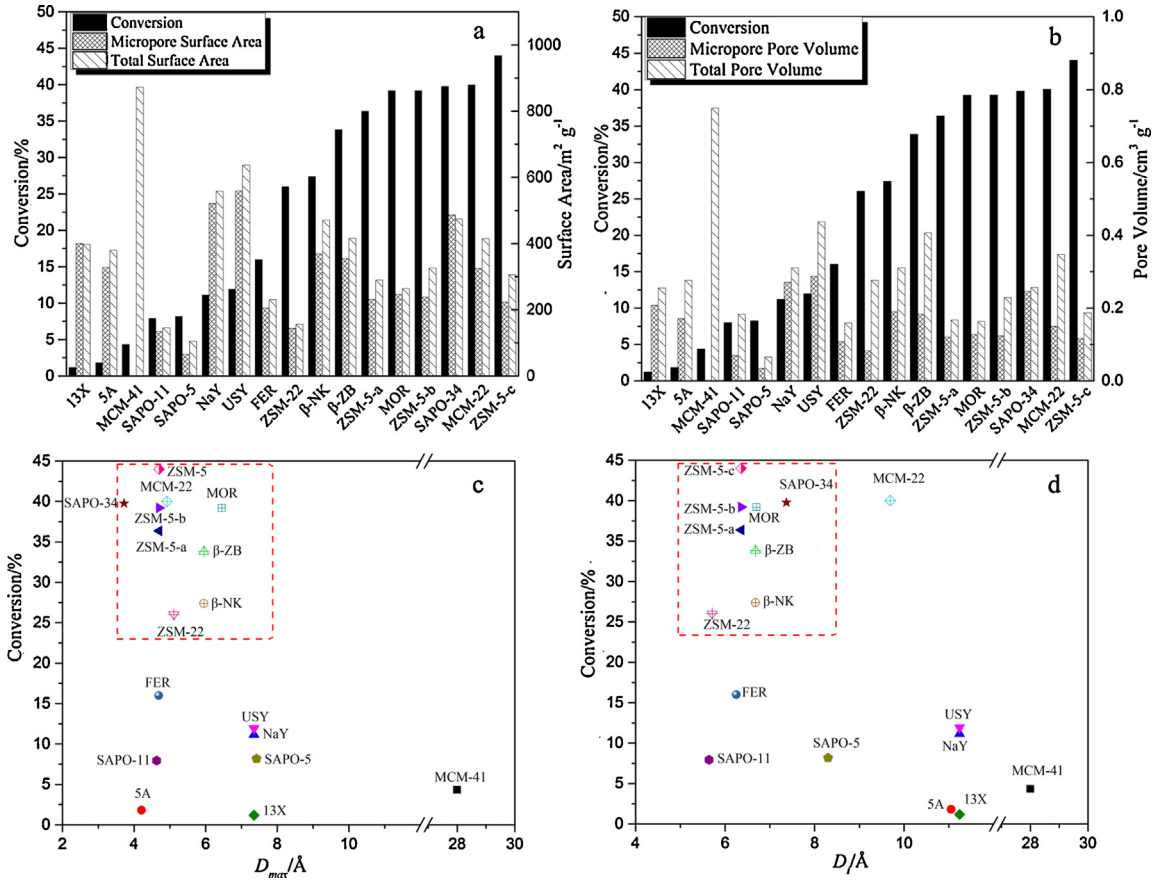

Fig. 3. Zeolite structure–NO conversion relationship versus: (a) total and micropore surface areas; (b) total and micropore pore volumes; (c) maximum free sphere diameter (D_{max}); and (d) maximum included sphere diameter (D_i).

relevant reactants and products to pass through the zeolite's channels resulting in the first selection rule for choosing zeolite catalysts for NO oxidation that D_{max} is not less than 3.46 Å.

As previously mentioned, D_i represents the largest spherical molecule that can fit in a zeolite cage with volume (V_{cage}) and should be investigated for its impact on NO oxidation (Fig. 3d). Steady-state NO conversion decreases with increasing D_i. However, MCM-22 and SAPO-11 are exceptions to this trend, having notably high and low conversions (40 and 7.9%, respectively). Effective zeolites with steady-state NO conversions ranging from 26.0 to 39.8% (e.g., ZSM-5, MOR, β, ZSM-22, and SAPO-34) have D_i values between 5.71 and 7.37 Å.

FER and ZSM-5 have similar D_i values (6.25 and 6.36 Å) and micropore volumes (0.159 and 0.167 $cm^3\,g^{-1}$), but at steady-state conditions, FER oxidizes 56% less NO than ZSM-5-a. This discrepancy may be attributed to topological differences. FER cages are circumscribed by eight ring channels along the *b*-axis (D_{max} = 3.40 Å, Fig. S1). These windows that provide the transitions between cages and channels may not be large enough to accommodate the TS formed or required for the oxidation reaction to proceed (this topic is described in more detail below). ZSM-5-a has a more reasonable D_{max} value (across all axes), allowing reactants/products/intermediates to be accommodated in cages and channels, allowing for higher steady-state NO conversion due to more effective utilization of void space. MCM-22 has surprisingly high conversion despite a large D_i (9.69 Å). Analyzing MCM-22 topology, it is observed that MCM-22 has a void space with an appropriate D_{max} (4.92 Å), which accounts for 45% of its void space [53], and 4.92 Å is in the range of D_{max} values for effective conversion. When predicting steady-state NO conversion, it is important to consider both channel and cage dimensions for zeolites that incorporate both structures.

The concentrated zone describing large NO conversions for ranges in D_i and D_{max} (Fig. 3), and interpretations for outliers, indicate that zeolites can be effective for NO oxidation if they have $4.70 < D_{max} < 6.45$ Å or $5.71 < D_i < 7.37$ Å.

It is also important to assess the relevance of pore volume to steady-state NO conversion. ZSM-5 after alkaline treatment provides a range of microporosity and mesoporosity values (Fig. 4). Since ZSM-5 has desirable D_i and D_{max} values, increasing the volume of active micropores (without altering their pore widths) is expected to increase steady-state NO conversion. Fig. 4a shows that increasing the zeolite's crystallinity and micropore volume cause increases in steady-state NO conversion (Table S3 and Fig. S6). Conversely, added mesoporosity does not improve a zeolite's steady-state NO conversion (Fig. 4b). It is expected that micropores are most active for NO oxidation, which is consistent with Artioli *et al.*'s [31] study showing that amorphous silica with mesoporosity is less effective than microporous zeolites (CHA, BEA, and SIL-1D). Large pore volume is expected to provide high conversion; however, increasing mesopore volume at the expense of micropore volume decreases conversions. The distinct increase in conversion for MCM-41 (D_i, 28 Å), NaY (D_i, 11.24 Å), and ZSM-5 (D_i, 6.36 Å) with pores changing from mesopores to micropores suggests that the influence of microporosity is more significant than that of mesoporosity, corroborating the findings on alkali-treated zeolites. Also, hydroxyl groups that were added during alkaline treatment do not increase the catalyst's conversion. Therefore, hydroxyl groups are

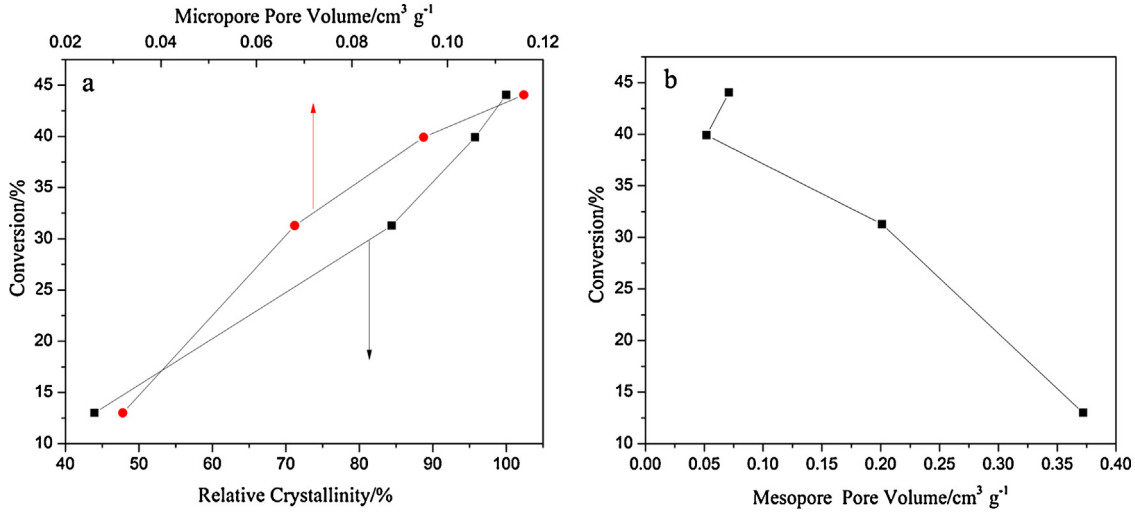

Fig. 4. NO conversion as a function of (a) relative crystallinity and micropore pore volume, and (b) mesopore pore volume of alkali-treated ZSM-5.

not required for zeolite-catalyzed NO oxidation [22,33], confirming earlier results that physical properties control steady-state NO conversion.

3.4. Comparisons between activated carbon fibers and zeolites

As previously mentioned, NO steady-state conversion by activated carbon fibers is mainly dependent on the physical properties of the catalysts [37]. In zeolites, D_i and D_{max}, combined with the distribution and volume of channels and cavities, determine the steady-state conversion of the catalyst. For activated carbon fibers, chemical properties including acidity surface functional groups and bulk composition impact transient oxidation kinetics without altering steady-state NO conversion and such property is consistent with observations for zeolites [34]. To highlight the similarities between the activated carbons and zeolites, pseudo-turnover frequency (TOF) was determined for the activated carbons and zeolites with small channel and/or cage widths (<7 Å). This calculation standardizes the catalysts' steady-state NO conversion by normalizing to micropore volumes. Despite the obvious chemical differences between carbon and zeolite materials (Table 1), the pseudo-TOF values are rather consistent for materials with similar channel/cage widths (Table 3). However, materials with larger channel and/or cage width (>7 Å) deviate from this trend. This observation suggests that a similar NO oxidation reaction mechanism exists for these two groups of catalysts and stresses that the physical properties, and not the chemical properties, of the catalyst control steady-state NO conversion.

Activated carbon fiber-catalyzed NO oxidation includes two consecutive steps: (1) rapid NO oxidation in micropores and (2) reactive adsorption of NO_2 onto the carbon surface. Similar pseudo-TOF values, NO_2 evolution profiles, and time scales for activated carbon and zeolites (Fig. S7) indicate that this mechanism could be consistent for the activated carbon fiber and zeolite materials tested here. Conversion associated with Step 1 is determined by the catalyst's physical properties, however, the reaction mechanism as to how physical properties impact the conversion is still not clear.

3.5. Transition state confinement mechanism

Gadzhiev *et al.* [39] reported that a two-step mechanism takes place entirely on the singlet state potential surface: (1) $2NO + O_2 \rightarrow TS1 \rightarrow CC$; (2) $CC \rightarrow TS2 \rightarrow 2NO_2$, where TS1 and TS2 are NO oxidation TSs and CC is a reaction intermediate. These authors also reported that the first step is rate-determining with an estimated activation energy of 6.67 kJ mol^{-1}, which is consistent with experimental activation energy values. These authors also suggested that the activation energy is greater than zero because of a basis set superposition error (BSSE) during simulation.

Increasing void space dimensions (i.e., D_{max} of zeolites where channels are dominant and D_i of zeolites where cages are dominant) beyond critical ranges in zeolites decreases NO conversion, highlighting the importance of adsorbate–adsorbent interaction. Non-specific van der Waals interaction is highest when the dimensions of the adsorbate closely match that of the accommodating void space. Increasing the dimensions of void space correspondingly weakens the van der Waals interaction between TS and pore walls of the zeolites, decreasing the catalyst's steady-state NO conversion. Results here are combined with quantum simulations from others [39] to propose TS1 as the TS for NO oxidation and to determine its associated free energy. The free energy of TS1 depends on the pore width of activated carbons and the channel/cage width of zeolites. Altering the channel/cage width of void spaces changes the activation energy required to form TS1 and correspondingly affects Step 1 of the reaction mechanism and its associated steady-state NO conversion. This concept of catalytic activity based on TS confinement in void spaces has been widely reported for hydrocarbon carbonylation, cracking, and dehydrogenation [54,55]. The mechanism proposed in this study is primarily based on Gadzhiev *et al.*'s research [39]. However, Artioli *et al.* recently proposed a confinement mechanism for NO oxidation catalyzed by select zeolites by means of kinetic and thermodynamic analyses, based on two different homogenous routes [56].

The estimated volume of TS1 is 70.1 Å^3 [36] and the corresponding spatial configuration of atoms is shown in Fig. 5. TS1 is three-dimensional with dimensions of 6.94 Å × 4.67 Å × 4.46 Å, along the *x*-, *y*-, and *z*-axes, respectively (Table S4). Reported zeolites with high conversion (25–40% for conditions tested here) have channels or cages that accommodate TS1, including ZSM-5 (6.36 Å and 135 Å^3, cage width and volume), SAPO-34 (7.37 Å and 209 Å^3), MOR (6.70 Å and 157 Å^3), ZSM-22 (5.71 Å and 97.4 Å^3), and β (6.68 Å and 156 Å^3) [44].

It is notable that the channels of SAPO-34 are smaller than TS1, yet the catalyst shows high steady-state NO conversion (40%). It is proposed that NO and O_2 diffuse through the zeolite's narrow channels and into the more accommodating cages, where TS1 can freely form. NO and O_2 do not readily react in SAPO-34 channels because they are too narrow for TS1. After the reaction occurs in

Table 3
Micropore volume, NO conversion, and pseudo-turnover frequency (pseudo-TOF)[a] values for zeolites and activated carbon fiber cloth (ACFC) at 50 °C.

	ZSM-22	MOR	ZSM-5-a	USY	ACFC-10[b]
Micropore volume ($cm^3\ g^{-1}$)	0.08	0.13	0.12	0.29	0.40
Conversion (%)	11.6	15.5	12.4	4.6	57
Reaction Rate ($\mu mol\ g^{-1}\ h^{-1}$)	49.9	66.4	53.3	19.8	232
Pseudo TOF ($\mu mol\ h^{-1}\ cm^{-3}$)	608	523	444	69	577

[a] Pseudo TOF = pseudo turnover frequency = reaction rate/micropore volume at steady-state conditions.
[b] NO conversion of ACFC-10 was obtained elsewhere [38]

the cages, the NO_2 product diffuses back through the channels and is released. The same argument can be made for zeolite 5A, where narrow channels again prevent TS1 formation while allowing for diffusion of the reactants. However, in 5A (Table 2), the cages are too large to provide van der Waals interaction between the TS and the pore walls of the zeolite necessary for the reaction to proceed, preventing any notable oxidation. SAPO-34 and 5A provide a valuable comparison between zeolites with variable cage sizes and highlight the importance of van der Waals interactions to form TS1–void spaces that are too small or too large are not effective for NO oxidation. These results also suggest that the TS is formed directly in the void space, rather than forming in the bulk gas phase and then transported to the more reactive void space. This direct formation of TS1 is expected to occur in channels or cages, if they are of appropriate dimensions.

Fig. 5 also describes reaction pathways for uncatalyzed (Route (1)) and catalyzed (Route (2)) NO oxidation. For Route (1), TS1 is formed slowly with an increased energy barrier, not benefitting from van der Waals interaction between TS and pore walls of the zeolites that is provided in the confined configurations. The energy barrier for generating TS1 in Route (2) is decreased due to being confined in a void space and the corresponding van der Waals interaction between TS1 and the pore walls of the zeolite.

The following discussion is to assist in describing the experimental trends described above. According to transition state theory [57], reaction rates depend on the decomposition of TS1. Eqs. (3)–(6) show the reaction rates and rate constants for uncatalyzed and zeolite-catalyzed NO oxidation, respectively (details in supporting information):

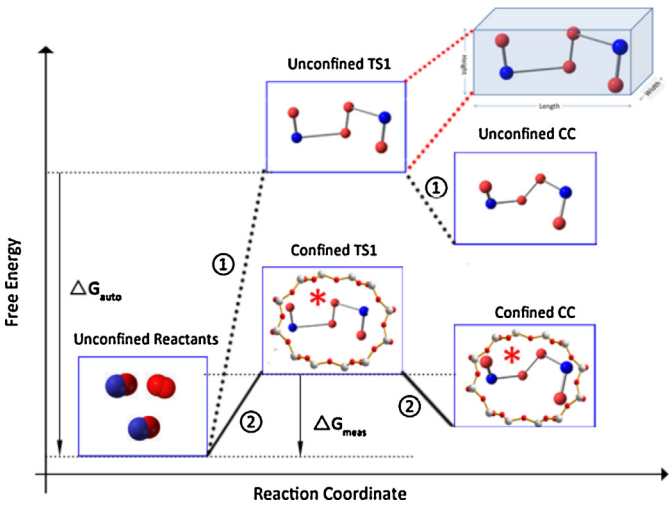

Fig. 5. Proposed reaction mechanism for NO oxidation. Route (1) represents the uncatalyzed oxidation pathway. Route (2) represents the pathway in the presence of zeolites. The inset describes the 3D spatial configuration of transient state derived from simulation, where red spheres represent oxygen and blue spheres represent nitrogen. The structures in shaded box is the TS with length, width, and height dimensions. ΔG_{meas} and ΔG_{auto} represent the differences between reactants and either confined TS and unconfined TS. Confined TS, marked with asterisk, indicates that the spatial configuration of TS is different from unconfined TS in spite of the same geometries shown in this figure.

$$r_1 = k_1[NO]^2[O_2] \tag{3}$$

$$k_1 = \frac{2k_BT}{h}\exp\left(-\frac{DG_{TS1} - 2DG_{NO} - DG_{O_2}}{RT}\right) \tag{4}$$

$$r_2 = k_2[NO]^2[O_2] * C_{space} \tag{5}$$

$$k_2 = \frac{2k_BT}{h}\exp\left(-\left(\frac{DG_{TS1(Z)} - 2DG_{NO} - DG_{O_2}}{RT}\right)\right) \tag{6}$$

where r_1 and r_2 are the corresponding reaction rates in the absence or presence of the zeolite catalyst, respectively, k_B is Boltzmann's constant, h is Planck's constant, T is the reaction temperature, and R is the ideal gas law constant. $DG_{TS1(Z)}$, DG_{NO} and DG_{O_2} represent the Gibbs free energy of the TS confined in zeolites, NO reactant, and O_2 reactant, respectively; DG_{TS1} represents the Gibbs free energy of TS in uncatalyzed scenarios. C_{space} is the number of active, catalytic sites per unit mass of zeolite.

Differences in reaction rates for the two routes are attributed to C_{space} and $DG_{TS1(Z)}$. Likewise, the rate constants for the two scenarios differ due to variability in TS1's Gibbs free energy. Steady-state NO conversion decreases with decreasing micropore volume (Fig. 4). This is consistent with the Eqs. (5) and (6). While C_{space} is dependent on effective pore volume or availability of effective void space for NO oxidation, $DG_{TS1(Z)}$ is dependent on the dimensional size of the void space relative to the size of TS1.

It is important to *quantify* the activation energy for these pathways, in addition to *qualifying* the impact of the catalyst's physical structure. Born–Haber thermochemical cycles [54] separate activation energy into enthalpy differences that independently reflect the properties of the reactants and catalysts, allowing isolation of the role of zeolite pore structure on NO reaction rates.

As previously mentioned, Fig. 6 shows two hypothetical pathways (solid red arrows) to approach a confined TS1, based on Born–Haber thermochemical cycles. The first approach (uncatalyzed) begins with TS1 generation in the bulk gas phase followed by transport to and adsorption in zeolite void spaces. The second approach (catalyzed) generates TS1 directly in the void space, where it is confined. E_{auto} (uncatalyzed) and $E_{w/c}$ (catalyzed) describe the activation energies of the two pathways, respectively:

$$E_{auto} + D_rH_{mads} = E_{w/c} \tag{7}$$

Because adsorption of TS1 is exothermic ($D_rH_{mads} < 0$), the catalyzed process has a lower activation energy by $|D_rH_{mads}|$.

Derouane *et al.* concluded that adsorption enthalpy ($|D_rH_m|$) is proportional to the van der Waals interaction ($W_r(s)$) of reactants and the zeolite's walls within void spaces [58]. The adsorption enthalpy can be expressed as

$$|D_rH_m| = \alpha W_r(s) = \frac{\alpha W(s)}{W(0)} = \alpha\left(1 - \frac{1}{2} * \frac{d_{mol}}{d_{zeo}}\right)^{-3} \tag{8}$$

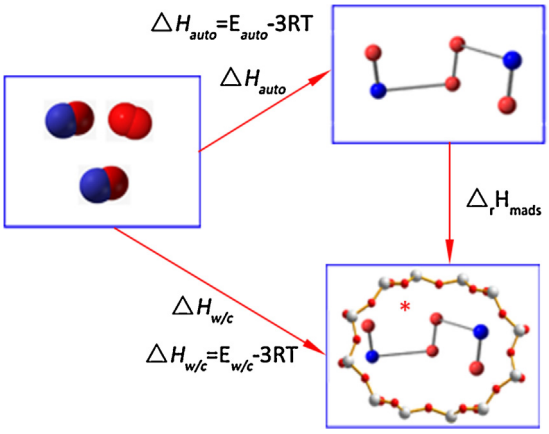

Fig. 6. Thermochemcial cycle for NO oxiation catalyzed with zeolites via [ONOONO] TS, the difference between activation energy (E_{auto} and $E_{w/c}$) and activation enthaply (ΔH_{auto} and $\Delta H_{w/c}$) is 3*RT* for homogeneous and hetergenous NO oxidation, and 3 is introduced because 3 is the number of molecules involoved in the formation of TS. Activation energy ($E_{w/c}$) depends on adsorption enthaplies ($\Delta_r H_{mads}$) of transitent state in void space and the intrinsic activation energy (E_{auto}) of NO homogenous oxidation.

$$E_{w/c} = E_{auto} - |D_r H_{mads}| = E_{auto} - \alpha W_r(s) = E_{auto} - \frac{\alpha W(s)}{W(0)} = E_{auto} - \alpha\left(1 - \frac{1}{2} * \frac{d_{mol}}{d_{zeo}}\right)^{-3} \quad (9)$$

where α is a constant, d_{mol} is the diameter of TS1, and d_{zeo} is the diameter of the considered void space. For results presented in this paper, activation energy is different for each zeolite because of variability in d_{zeo}, which also causes variability in reaction rates according to Arrhenius's law [57]. Zeolites such as 13X, NaY, and MCM-41 show lower conversion due to larger d_{zeo}. Zeolites with d_{zeo} close to d_{mol}, such as SAPO-34, MCM-22, MOR, ZSM-5, β, and ZSM-22, yield higher conversion due to lower (more negative) activation energy.

Combining Eqs. (5), (6) and (9), and Gibbs free energy equation allows for determination of reaction rate constants as a function of zeolite void space properties:

$$r_2 = \frac{2k_B T}{h} e^3 \exp\left(\frac{DS_{auto} + DS_{mads}}{R}\right) \exp\left(-\frac{E_{auto}}{RT}\right) \times \exp\left(\frac{\alpha(1 - 1/2 * (d_{mol})/(d_{zeo}))^{-3}}{RT}\right) [NO]^2 [O_2] * C_{space} \quad (10)$$

where DS_{auto} is the entropy of Route (1), and DS_{mads} is the entropy of TS adsorption in void space (Fig. 5).

Artioli *et al.* reported that zeolite-catalyzed NO oxidation yields negative enthalpies of formation for TS (−31 to −41.2 kJ mol^{-1}), and negative entropies of formation (−262.3 to −309.2 J mol^{-1} K^{-1}) with respect to the gaseous reactants [31]. The authors stated that the contribution of these entropy losses to the decrease of Gibbs free energy, along with enthalpic stabilization, are less consequential at ambient temperatures [31,34,55]. In light of the non-uniform pore widths, Eq. (3) can be modified to account for non-uniform pore widths, as described below:

$$r_2 = \frac{2k_B T}{h} e^3 \exp\left(\frac{-E_{auto}}{RT}\right) [NO]^2 [O_2] \sum_{i=1}^{n} \times \exp\left(\frac{DS_{auto} + DS^i_{mads}}{R}\right) \exp\left(\frac{\alpha(1 - 1/2 * (d_{mol})/(d^i_{zeo}))^{-3}}{RT}\right) * C^i_{space} \quad (11)$$

Table 4
Length scales of reactants, products, transition state, D_{max}, and D_i for zeolites, pore width for carbon, and recommended size for NO oxidation.

Items	Scale (Å)
Reactants	NO: 3.17, O_2: 3.46
Products	NO_2: 3.40
Dimensional size of transition state	6.94 × 4.67 × 4.46
Maximum free sphere diameter (D_{max})	4.70 < D_{max} < 6.45
Maximum included sphere diameter (D_i)	5.71 < D_i < 7.37
Appropriate pore width for activated carbon fibers	7
Recommended size for NO oxidation	4.67–6.94

where i = 1–n, and n is the total number of pore width type available in zeolites.

Eq. (11) explains the NO oxidation mechanisms that have been described in the literature, including: (1) increased conversion with increasing [NO] or [O_2], (2) negative activation energy, (3) higher conversion with increasing micropore volume, and (4) NO conversion's dependence on pore width. Eq. (11) explains notable trends that have been reported for NO oxidation catalyzed by microporous materials (including activated carbons and zeolites). Note that Eq. (11) is derived based only on the forward reaction rate and does not consider reverse reactions or the influence of NO_2 inhibition. Kinetic studies with quantitative analyses to estimate thermodynamic values should be completed in future NO oxidation studies, especially for zeolites with high NO_x adsorption capacity (e.g., NaY and 13X).

3.6. Extending results to other zeolite catalysts

It is challenging to test all 206 zeolite framework structures to determine those with high conversion. Instead, results presented here allow us to minimize the number of experiments by focusing only on zeolites that are predicted to perform well. Zeolites with high conversion should: (1) have channels ≥3.46 Å that accommodate all reactants (NO and O_2) and products (NO_2), (2) have void spaces (channels or cages) ≥4.67 Å that accommodate TS1, (3) have void spaces ≤6.94 Å that accommodate largest length scale for TS, maximizes van der Waals interaction between TS and the pore walls of the zeolite, and minimizes activation energy, and (4) if the cage size is <6.94 Å, have channels not <4.67 Å. These two boundaries (4.67 and 6.94 Å) are derived from TS calculations and summarized in Table 4.

Adhering to these criteria, zeolite structures that will be effective NO oxidation catalysts were predicted (Fig. 7 and Table 5). Zeolites with potentially high NO conversion are concentrated between two horizontal lines (D_i = 4.67 and 6.94). This analysis decreases the number of possible zeolites that should be tested as

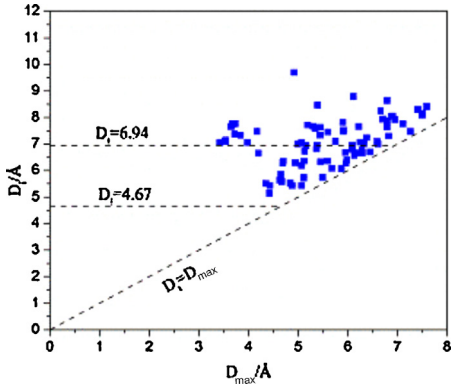

Fig. 7. Preferred zeolites for NO oxidation from International Zeolite Association; squares represent zeolites with the specified values for D_i and D_{max}.

Table 5
Select zeolites for NO oxidation from International Zeolite Association [32].

Code	AEI	AEL	AWW	*BEA	AFO	AFT	AFX	AFY	ASV	STI	*STO	STW	−SVR
D_i (Å)	7.33	5.64	7.48	6.68	5.43	7.75	7.76	7.82	5.43	6.29	6.8	5.43	5.85
D_{max} (Å)	3.84	4.63	4.17	5.95	5.07	3.68	3.73	5.9	4.43	4.94	6.09	4.88	4.65

Code	ATO	ATS	DDR	EAB	BEC	BOF	BOG	CAN	CFI	SZR	TER	TON	TUN
D_i (Å)	5.74	7.30	7.66	7.14	6.95	5.58	8.05	6.27	7.47	6.27	6.94	5.71	8.46
D_{max} (Å)	5.49	6.82	3.65	3.54	6.09	4.67	6.88	5.96	7.26	4.69	5.16	5.11	5.39

Code	CHA	CON	IFR	IMF	EON	ERI	EUO	EZT	FER	USI	UWY	VET	−WEN
D_i (Å)	7.37	7.45	7.24	7.34	7.87	7.04	7	6.57	6.31	6.76	8.78	6.39	5.53
D_{max} (Å)	3.72	5.6	6.38	5.44	6.79	3.42	4.99	6.13	4.69	6.28	6.11	5.98	4.84

Code	GME	GON	LTF	MAZ	ISV	ITH	ITR	IWR	IWS	SFE	SFF	SFG	SFH
D_i (Å)	7.76	6.32	8.16	8.09	7.01	6.72	6.36	7.48	8.25	6.66	7.59	6.96	7.63
D_{max} (Å)	7.11	5.45	7.5	7.5	6.32	5.13	5.12	5.91	6.66	6.29	5.34	5.38	6.79

Code	IWW	LEV	MSE	MTT	MEI	MEL	MER	MFI	MFS	SFN	SFO	SFS	*SFV
D_i (Å)	7.07	7.1	7.09	6.19	8.06	7.72	6.65	6.36	6.81	7.94	7.92	7.52	7.67
D_{max} (Å)	6.25	3.53	6.59	5.07	6.9	5.19	4.2	4.7	5.37	6.7	6.95	5.92	5.3

Code	MOR	MRE	PUN	−RON	MTW	MWW	NES	OFF	RTE	STF	SOF	SSF	SSY
D_i (Å)	6.7	6.36	5.51	5.74	6.08	9.69	7.04	7	7.06	7.63	5.14	7.66	7.1
D_{max} (Å)	6.45	5.59	4.35	5.11	5.68	4.92	5.07	6.61	3.98	5.44	4.42	6.22	5.75

Code	OSI	OSO	SAF	SAO
D_i (Å)	6.66	6.07	6.66	8.64
D_{max} (Å)	6.28	5.87	6.19	6.79

NO oxidation catalysts from 206 codes to 82 codes. This screening from International Zeolite Association (IZA) database is based on D_i and D_{max}, and later achieved based on the accessibility of void space and diffusion. In the future, more comprehensive/precise descriptors should be developed that represent the size and volume of combined void spaces (not exclusively windows or cavities). While the reliance on D_i or D_{max} rationalizes most of the experimental results described in this study, improvements could be made by using a more generic term to describe the dominant properties and abundance to cause NO oxidation. Other investigators are developing methods to determine such parameters [53,59], and these studies will be instrumental in identifying a more comprehensive/precise method to predict NO conversion achieved by zeolite catalysts.

4. Summary and conclusions

Experimental screening shows that zeolite-catalyzed steady-state NO conversion is not strongly related to the catalyst's chemical composition, including surface hydroxyl groups and Si/Al ratio, but strongly depends on the catalysts' void space dimensions and concentrations. Chemical properties are shown to impact transient oxidation kinetics before approaching stable NO concentration, which is consistent with previous studies describing carbonaceous NO oxidation catalysts. A zeolite-catalyzed NO oxidation mechanism is proposed, based on both experimental results and quantum mechanical studies, which better accounts for trends that had previously not been justified in the literature. In particular, the mechanism describes the impact of void space dimensions and volumes. The mechanism provides a pathway where transition state 1 (TS1) is generated and confined in void spaces. Lowest activation energy and high reaction rates, influenced by the dimensions of void spaces, are achieved in the effective void space with dimensions ranging between 4.67 and 6.94 Å, consistent with reported results for activated carbon fibers. The mechanisms for activated carbon fiber cloth and zeolites confirm that steady-state NO conversion is mainly dependent on the catalyst's physical properties. Engineering materials with appropriate pore width and large micropore volume in the range of appropriate pore width presumably renders high conversion of NO oxidation. This provides the background needed to more effectively investigate select zeolites and carbons as NO oxidation catalysts, as well as other unique materials that have not yet been considered for these reactions (e.g., metal organic frameworks).

Acknowledgements

Funding was provided by the United States' National Science Foundation (NSF A1918 and NSF CBET 10-34470), and Zhejiang Provincial Natural Science Foundation of China (LY14E080001). Support for Z. Zhang was provided by Chinese Scholarship Council (2011645015). X-ray diffraction was carried out in the Frederick Seitz Materials Research Laboratory Central Facilities, University of Illinois, which are partially supported by the U.S. Department of Energy under grants DE-FG02-07ER46453 and DE-FG02-07ER46471. Zeolyst, Nanki Catalyst Company, and Jiangge Hao of Tianjin University are acknowledged for providing the tested zeolites. Jinyang Xi of Tsinghua University is acknowledged for calculating the transition state volume, and Dr. Phillip H. Geil of UIUC is acknowledged for providing the hydraulic press used for catalyst preparation.

Appendix A. Supplementary data

Supplementary material related to this article can be found, in the online version, at http://dx.doi.org/10.1016/j.apcatb.2014.06.044.

References

[1] G. Qi, R.T. Yang, R. Chang, Appl. Catal. B 51 (2004) 93–106.
[2] Z. Zeng, P. Lu, C. Li, L. Mai, Z. Li, Y. Zhang, Catal. Sci. Technol. 2 (2012) 2188–2199.

[3] Q.P. Wu, G. Mul, R. van de Krol, Energy Environ. Sci. 4 (2011) 2140–2144.
[4] Environmental Protection Ministry PRC, Waste gas, Ministry of Environmental Protection, PRC, Retrieved 12 May 2013, from http://zls.mep.gov.cn/hjtj/nb/2010tjnb/201201/t20120118_222725.htm
[5] State Council, Energy Conservation and Emissions Reduction in 12th Five Year Plan, China New Energy Website, Retrieved 12 May 2013, from http://www.china-nengyuan.com/news/37608.html
[6] S. Brandenberger, O. Kröcher, A. Tissler, R. Althoff, Catal. Rev. 50 (2008) 492–531.
[7] M. Shelef, Chem. Rev. (Washington, DC, U.S.) 95 (1995) 209–225.
[8] W.J. Zhang, S. Rabiei, A. Bagreev, M.S. Zhuang, F. Rasouli, Appl. Catal. B 83 (2008) 63–71.
[9] J.F. Brilhac, A. Sultana, P. Gilot, J.A. Martens, Environ. Sci. Technol. 36 (2002) 1136–1140.
[10] X. Chang, G. Lu, Y. Guo, Y. Wang, Y. Guo, Micro. Meso. Mater. 165 (2013) 113–120.
[11] S. Liu, Fundamental research on removal of SO_2 over activated carbon and metal doped carbon, Zhejiang University, Zhejiang, 2011.
[12] J.D. Atkinson, Z.Q. Zhang, Z.F. Yan, M.J. Rood, Carbon 54 (2013) 444–453.
[13] I. Mochida, Y. Kawabuchi, S. Kawano, Y. Matsumura, M. Yoshikawa, Fuel 76 (1997) 543–548.
[14] I. Mochida, S. Kisamori, M. Hironaka, S. Kawano, Y. Matsumura, M. Yoshikawa, Energy Fuels 8 (1994) 1341–1344.
[15] I. Mochida, N. Shirahama, S. Kawano, Y. Korai, A. Yasutake, M. Tanoura, S. Fujii, M. Yoshikawa, Fuel 79 (2000) 1713–1723.
[16] J.P.S. Sousa, M.F.R. Pereira, J.L. Figueiredo, Catal. Today 176 (2011) 383–387.
[17] J.P.S. Sousa, M.F.R. Pereira, J.L. Figueiredo, Appl. Catal. B 125 (2012) 398–408.
[18] S. Sumathi, S. Bhatia, K.T. Lee, A.R. Mohamed, Chem. Eng. J. (Lausanne) 162 (2010) 51–57.
[19] S. Sumathi, S. Bhatia, K.T. Lee, A.R. Mohamed, J. Hazard. Mater. 176 (2010) 1093–1096.
[20] Y.F. Li, H.Y. Liu, H.F. Huang, H.F. Lu, Y.F. Chen, Chin. Environ. Sci. 30 (2010) 161–166.
[21] Y.F. Li, H.Y. Liu, H.F. Huang, Z.K. Zhang, Y.F. Chen, Chin. Environ. Sci. 29 (2009) 469–473.
[22] H. Liu, Z. Zhang, Y. Xu, Y. Chen, X. Li, Chin. J. Catal. 31 (2010) 1233–1241.
[23] H.Y. Liu, Y.F. Li, Y.Y. Xu, Y.F. Chen, X. Li, J. Chem. Eng. Chin. Univ. 25 (2011) 615–621.
[24] Na Xing, Xinping Wang, X. Qing Yu, Guo, Chin. J. Catal. 28 (2007) 205–209.
[25] J. Despres, M. Koebel, O. Kröcher, M. Elsener, A. Wokaun, Micro. Meso. Mater. 58 (2003) 175–183.
[26] Y. Wang, Z. Lei, B. Chen, Q. Guo, N. Liu, Appl. Surf. Sci. 256 (2010) 4042–4047.
[27] D.J. Kang, X. Tang, J. Peng, H. Yi, P. Ni, K. Ye Zhiqing, Li, Adv. Mater. Res. 383–390 (2011) 3056–3062.
[28] S.E. Schwartz, W.H. White, Solubility Equilibria of the Nitrogen Oxides and Oxyacids in Dilute Aqueous Solution, Gordon and Breach Science Publishers, New York, NY, 1981.
[29] J.H. Seinfeld, Atmospheric Chemistry and Physics of Air Pollution, Wiley-Interscience, New York, 1986.
[30] P. Nowicki, R. Pietrzak, Chem. Eng. J. (Lausanne) 166 (2011) 1039–1043.
[31] N. Artioli, R.F. Lobo, E. Iglesia, J. Phys. Chem. C 117 (2013) 20666–20674.
[32] M. Richter, R. Eckelt, B. Parlitz, R. Fricke, Appl. Catal. B 15 (1998) 129–146.
[33] I. Halasz, A. Brenner, K.Y. Simon Ng, Catal. Lett. 34 (1995) 151–161.
[34] J.A. Loiland, R.F. Lobo, J. Catal. 311 (2014) 412–423.
[35] Ch. Baerlocher and L.B. McCusker, Database of Zeolite Structures. http://www.iza-structure.org/databases/
[36] M.D. Foster, M.M.J. Treacy, A database of hypothetical zeolite structures. http://www.hypotheticalzeolites.net
[37] Z. Zhang, J.D. Atkinson, B. Jiang, M.J. Rood, Z. Yan, Appl. Catal. B 148–149 (2014) 573–581.
[38] J.D. Atkinson, Z. Zhang, M.J. Rood, Impact of Carbon's Porosity and Surface Chemistry on NO oxidation Efficiency, in: 105th Air & Waste Management Association Conference, San Antonio, 2012, Paper 2012-A-2058-AWMA.
[39] O.B. Gadzhiev, S.K. Ignatov, S.A. Gangopadhyay, M.E. Masunov, A.I. Petrov, J. Chem. Theory Comput. 7 (2011) 2021–2024.
[40] Q. Zhang, C. Li, H. Shan, C. Yang, Chem. J. Chin. Univ. 32 (2011) 2721–2726.
[41] C.-M. Song, J. Jiang, Z.-f. Yan, J. Porous Mater. 15 (2008) 205–211.
[42] C. Fernandez, I. Stan, J.-P. Gilson, K. Thomas, A. Vicente, A. Bonilla, J. Pérez-Ramírez, Chem. Eur. J. 16 (2010) 6224–6233.
[43] Test Method for Determination of Relative Crystallinity of Zeolite ZSM-5 by X-Ray Diffraction, ASTM International, 2001.
[44] M.M.J. Treacy, M.D. Foster, Micro. Meso. Mater. 118 (2009) 106–114.
[45] G.W.T.M.J. Frisch, H.B. Schlegel, G.E. Scuseria, M.A. Robb, J.R. Cheeseman, G. Scalmani, V. Barone, B. Mennucci, G.A. Petersson, H. Nakatsuji, M. Caricato, X. Li, H.P. Hratchian, A.F. Izmaylov, J. Bloino, G. Zheng, J.L. Sonnenberg, M. Hada, M. Ehara, K. Toyota, R. Fukuda, J. Hasegawa, M. Ishida, T. Nakajima, Y. Honda, O. Kitao, H. Nakai, T. Vreven, J.A. Montgomery Jr., J.E. Peralta, F. Ogliaro, M. Bearpark, J.J. Heyd, E. Brothers, K.N. Kudin, V.N. Staroverov, R. Kobayashi, J. Normand, K. Raghavachari, A. Rendell, J.C. Burant, S.S. Iyengar, J. Tomasi, M. Cossi, N. Rega, J.M. Millam, M. Klene, J.E. Knox, J.B. Cross, V. Bakken, C. Adamo, J. Jaramillo, R. Gomperts, R.E. Stratmann, O. Yazyev, A.J. Austin, R. Cammi, C. Pomelli, J.W. Ochterski, R.L. Martin, K. Morokuma, V.G. Zakrzewski, G.A. Voth, P. Salvador, J.J. Dannenberg, S. Dapprich, A.D. Daniels, Ö. Farkas, J.B. Foresman, J.V. Ortiz, J. Cioslowski, D.J. Fox (Eds.), Gaussian 03, Revisions E.01, Gaussian, Inc., Wallingford, CT, 2004.
[46] S.S. Batsanov, Inorg. Mater. 37 (2001) 871–885.
[47] N. Tang, Y. Liu, H. Wang, Z. Wu, J. Phys. Chem. C 115 (2011) 8214–8220.
[48] Y. Yang, N. Burke, J. Zhang, S. Huang, S. Lim, Y. Zhu, RSC Adv. 4 (2014) 7279–7287.
[49] Z.-M. Wang, T. Arai, M. Kumagai, Energy Fuels 12 (1998) 1055–1060.
[50] Z. Zhang, J.D. Atkinson, H. Song, M.J. Rood, Z. Yan, Structure Sensitivities of SAPO Zeolites on Catalytic Oxidation of Nitric Oxide, in: 106th Air&Waste Management Association, Chicago, 2013, p. 12406.
[51] S. Smeekens, S. Heylen, N. Janssens, K. Houthoofd, J.A. Martens, C.E.A. Kirschhock, Chem. Mater. 23 (2011) 4606–4611.
[52] A.M. Rubel, J.M. Stencel, Energy Fuels 10 (1996) 704–708.
[53] E.L. First, C.E. Gounaris, J. Wei, C.A. Floudas, Phys. Chem. Chem. Phys. 13 (2011) 17339–17358.
[54] R. Gounder, E. Iglesia, J. Am. Chem. Soc. 131 (2009) 1958–1971.
[55] R. Gounder, E. Iglesia, Chem. Commun. (Cambridge, U.K.) 49 (2013) 3491–3509.
[56] H. Tsukahara, T. Ishida, M. Mayumi, Nitric Oxide 3 (1999) 191–198.
[57] X. Fu, W. Shen, t. Yao, W. Hou, Handbook of Physical Chemistry, High Education Press, Beijing, 2005.
[58] E.G. Derouane, J.-M. Andre, A.A. Lucas, J. Catal. 110 (1988) 58–73.
[59] A.J. Jones, C. Ostrouchov, M. Haranczyk, E. Iglesia, Micro. Meso. Mater. 181 (2013) 208–216.